PROCEEDINGS OF SCIENCE

The accurate measurement of pulse energy by pyroelectric energy sensors for LHAASO-WFCTA calibration

Lei Xie ,[a,*] Qinning Sun,[a] Yang Wang,[a] Long Chen,[a] Yong Zhang[b,c] and Fengrong Zhu[a,†] for the LHAASO collaboration

[a] *Southwest Jiaotong University, School of Physical Science and Technology, No.999, Xi'an Road, Chengdu, 611756, China.*

[b] *Key Laboratory of Particle Astrophysics & Experimental Physics Division & Computing Center, Institute of High Energy Physics, Chinese Academy of Sciences, 19B Yuquan Road, Beijing, 100049, China.*

[c] *TIANFU Cosmic Ray Research Center, Institute of HighEnergy Physics, Chinese Academy of Sciences, 1500 Kezhi Road, Chengdu, 610000, China.*

E-mail: zhufr@ihep.ac.cn

The Large High Altitude Air Shower Observatory (LHAASO), situated on Haizi Mountain in Daocheng County, Sichuan Province, at an average altitude of 4,410 meters, is home to the Wide Field-of-view Cherenkov Telescope Array (WFCTA), a critical component of which is the laser calibration systems (LCS). The energy measurement systems within the LCS are responsible for accurately measuring the energy of laser beams emitted to the field of view of WFCTA, and are comprised of an energy sensor, energy meter, and temperature control system. This paper presents the results of the relative calibration and performance testing of the energy sensor, which serve as the foundation for the normal operation of the LCS.

38th International Cosmic Ray Conference (ICRC2023)
26 July - 3 August, 2023
Nagoya, Japan

*Speaker

PoS(ICRC2023)496

1. Introduction

The Large High Altitude Air Shower Observatory (LHAASO) locates on Haizi Mountain in Daocheng, Sichuan Province, China, at an altitude of 4,410 m above sea level. It consists of three interconnected arrays of the Kilometer Square Array (KM2A), Water Cherenkov Detector Array (WCDA), and Wide Field-of-view Cherenkov Telescope Array (WFCTA)[1–3]. The WFCTA, consisting of 18 Cherenkov telescopes, is primarily utilized for the accurate measurement of cosmic ray components ranging from 10^{13} to 10^{18} eV[4]. The laser calibration systems (LCS), distributed at the edge of LHAASO, are crucial components of the WFCTA. Since November 2022, five sets of LCS have been constructed at LHAASO site, as depicted in Figure 1. Three nitrogen laser devices with a wavelength of 337.1 nm are deployed in L2, L4, and L5, while in L3, a single Nd:YAG laser device with a wavelength of 355 nm is employed. L1, which is not shown in Figure 1, is a mobile LCS located outside the LHAASO site[5, 6].

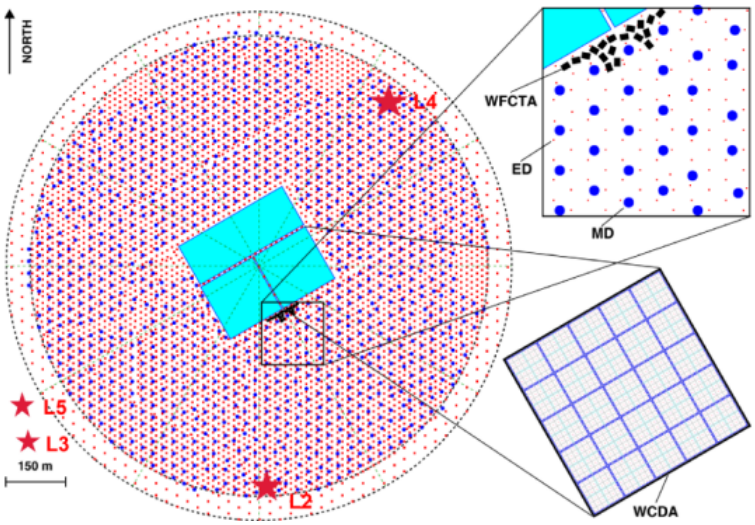

Figure 1: The schematic layout of LHAASO , with the stars indicating the location of the laser calibration systems (LCS). Specifically, L2, L3, L4, and L5 are situated at distances of 465 m, 1000 m, 650 m, and 1000 m from the WFCTA, respectively.

The LCS of WFCTA employ an end-to-end calibration method. Laser beams, which contain N_0 photons, are emitted from laser devices at a series of specific angles and across the field of view of the WFCTA[7]. Simultaneously, N_1 scattering photons, which are scattered by air molecules and aerosols, are received and recorded by the WFCTA. To calculate photon counts N_0, the energy measurement system is designed to measure the energy of the laser beams. This system comprises an energy sensor, an energy meter, and a temperature control system. The energy sensor and energy meter are the pyroelectric sensor (PE25-C) and ethernet adapter (EA) respectively, both produced by Ophir. Although the energy sensor is a commercial product, certain parameters require careful measurement. In this study, we performed relative calibration of the energy sensor and tested its performance, including the non-uniformity of the energy sensor, the response of the energy sensor to laser beams from various angles, and the temperature effect of the energy sensor. Our results indicate that the error associated with measuring laser energy using different batches of energy

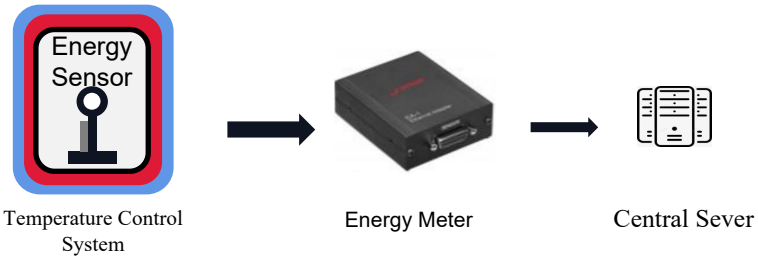

Figure 2: The schematic diagram of the energy measurement system utilized in the laser calibration systems. The energy sensor is connected to the energy meter, and the energy data is stored in the center server. The temperature control system comprises an aluminum shell (blue), an insulation layer (red), and a heating layer (black). The gray part attached to the energy sensor represents the temperature probe, which provides real-time feedback on the ambient temperature of the energy sensor.

sensors can be reduced by relative calibration between energy sensors. The maximum area of the energy sensor that meets the experimental requirements is 10 mm × 10 mm. The response non-uniformity of the energy sensor to laser beams from various angles can be ignored during calibration. The energy sensors exhibit a temperature effect, and this effect cannot be disregarded.

2. The relative calibration of energy sensor

In this study, the energy sensor (S/N:942580) was calibrated using a calibrated laser device supplied by the National Institute of Metrology of China (NIM) to obtain the correction factor of the energy sensor. The computational formula for the correction factor is shown in equation 1.

$$\text{Factor} = \frac{E_0}{E} \tag{1}$$

,where E_0 is the standard energy emitted by the calibrated laser device, and E is the reading of the energy sensor (S/N:942580). The correction factor for the energy sensor 942580 is 0.985, with a measurement uncertainty of 0.03. Experimental data presented in Table 1 demonstrate that different energy sensors yield varying results when used to measure the pulse energy of the same laser device.With the energy sensors 942580 as the standard energy sensor, the other sensors were relatively calibrated. The relative calibration coefficients for energy sensors 946780 and 3032620 are 1.06 and 1.10, respectively. By conducting relative calibration between energy sensors, the error associated with measuring laser energy using different batches of energy sensors can be reduced.

Serial Number (S/N)	Energy(μJ)	Relativecalibration
942580 *	123.6	1
946780	130.7	1.06
3032620	135.3	1.10

Table 1: Relative calibration of energy sensors and the star indicates the standard one.

3. Test of performance on energy sensor

3.1 The non-uniformity of the energy sensor aperture

In this section, we designed a two-dimensional scanning experiment to assess the non-uniformity of the aperture surface of the energy sensor. The experiment involved fixing the energy sensor onto a two-dimensional moving platform, which enabled us to control the movement of the energy sensor and the beam size on its aperture surface. The scanning path, as demonstrated in figure 3, was sequential from left to right and from top to bottom, with a scanning step length of 2 mm. To account for the rectangular shape of the beam size, which is 3 mm × 4 mm, we selected a rectangular area to scan the aperture surface of the energy sensor. Specifically, the black, purple, red, and blue areas in figure 3 have side lengths of 14 mm, 10 mm, 6 mm, and 2 mm, respectively. For each area, we measured 49, 25, 9, and 1 positions, respectively. The non-uniformity was calculated using equation 2.

$$U = \pm \frac{E_{max} - E_{min}}{2 \times E_{mean}} \times 100\,\% \tag{2}$$

, where E_{max}, E_{min}, and E_{mean} represent the maximum, minimum, and average values of laser pulse energy over all positions in the scanned areas. The non-uniformity of the aperture surface is presented in Table 2 for the black, purple and red areas. We found that the maximum area of the energy sensor that meets the experimental requirements is 10 mm × 10 mm, with the non-uniformity of ± 0.53 %.

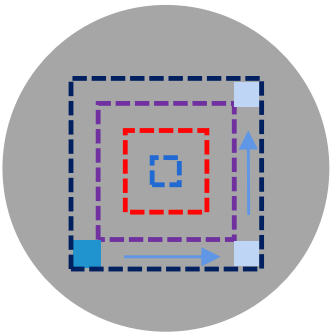

Figure 3: The schematic diagram of 2D scanning for measuring non-uniformity.

Rectangular Area	Non-uniformity
6 mm × 6 mm	± 0.23 %
10 mm × 10 mm	± 0.53 %
14 mm × 14 mm	± 1.19 %

Table 2: The non-uniformity of energy sensor by 2D scanning.

3.2 The non-uniformity response of the energy sensors to laser beams from various angles

The aperture surface of the energy sensor comprises a metal surface with a reflectance of 50 %. If the laser is incident vertically on the energy sensor, the laser beam is reflected back to the laser

exit window, potentially leading to damage of the laser device. Therefore, it is recommended to ensure a certain incident angle $\Delta\theta$ between the incident direction and the normal of the energy sensor during installation to prevent such damage. In this study, we designed an experiment to investigate the impact of the incidence angle $\Delta\theta$ on the energy sensor.

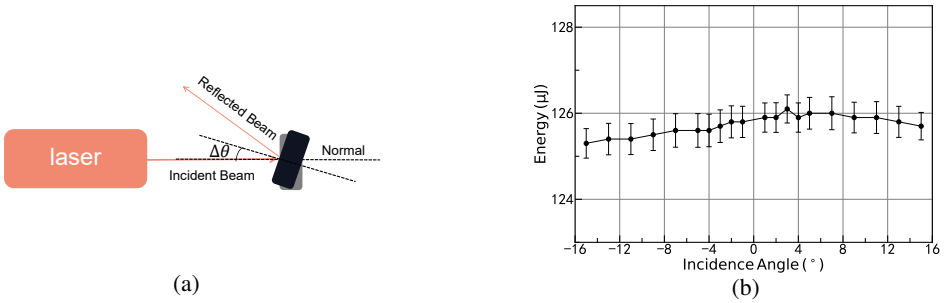

Figure 4: The experimental diagram and the relationship between the laser beam incidence direction and the reading of the energy sensor.

The energy sensor was affixed to a rotational stage and subsequently adjusted to ensure that the laser beam was directed towards the center of the energy sensor. The stage was then rotated to change the angle, $\Delta\theta$, between the incident direction of the laser beam and the normal of the surface, as depicted in figure 4(a). The relationship between the direction of laser beam incidence and the energy sensor reading was illustrated in figure 4(b). As the laser incidence angle increased, the reading of the energy sensor decreased. However, the reading deviation of $-9°$ to $9°$ was only 0.45 %, which was deemed negligible for calibration purposes since the experiment necessitates that the measurement error of laser pulse energy be limited to less than 2%[6].

3.3 The temperature effect of energy sensor

The PE25-C energy sensor is designed to operate based on pyroelectric effects. It has been discovered that pyroelectric materials exhibit piezoelectric properties, whereby the thermal expansion and contraction of the material generates electrons. This pyroelectric effect, known as the secondary pyroelectric effect, is caused by the thermal expansion of materials[8]. Thus, the PE25-C energy sensor possesses temperature-sensitive characteristics.

To conduct temperature effect experiments, a temperature control chamber is required to facilitate changes in the environmental temperature. During the experiment, both the energy sensor and meter are placed inside the chamber, which modifies the temperature surrounding the energy sensor. Meanwhile, the laser, which is kept at a constant temperature, is positioned outside the chamber. The laser beam is directed into the chamber through an observation port and directed towards the energy sensor.

It is worth noting that the temperature at LHAASO fluctuates rapidly, with temperatures dropping as low as $-27\,°$C. Figure 5 displays the temperature changes both inside and outside the calibration room from 7 pm to 7 am during the 2021-2022 observation season. The outdoor temperature varies from $-25°$C to 20°C, whereas the temperature range in the laser calibration room spans from $-15°$C to 20°C. Therefore, this range was chosen for our experiment accordingly.

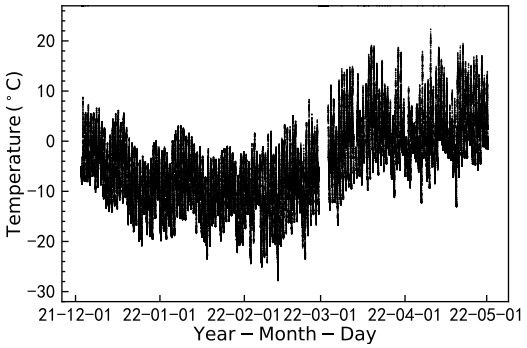

Figure 5: The temperature changes in LHAASO site.

The experimental results are presented in figure 6. As the environmental temperature increases from −15°C to 20°C, the reading of the energy sensor decreases by 1.5%. A linear approximation can be employed to describe the correlation between energy sensor readings (E) and temperature (T), which can be expressed as:

$$E(T) = -7.02 \times 10^{-2} T + 130.3 \tag{3}$$

These findings indicate that the energy probe is indeed susceptible to temperature effects. Based on the results of our temperature effect on the energy probe, it was observed that the energy of laser pulses exhibits a linear decline trend with increasing temperature. This finding can be utilized to rectify the photon counts acquired at varying temperatures, which is of paramount importance for the precision of our laser calibration.

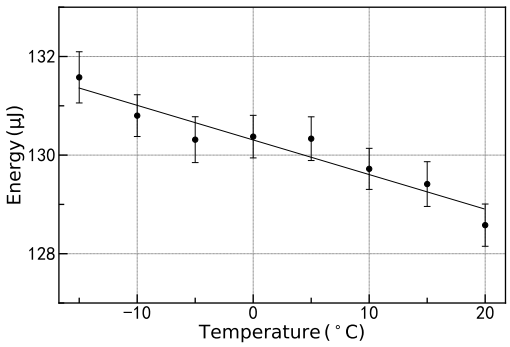

Figure 6: The temperature effect results.

4. Summary

This paper introduces the energy measurement system of LCS and presents the results of relative calibration and the performance testing of the energy sensor used in the system. By conducting relative calibration between energy sensors, the error associated with measuring laser energy using different batches of energy sensors can be reduced. The findings reveal that the optimal sensor area

for the experiment is 10 mm × 10 mm. Furthermore, the response of the energy sensors to laser beams from various angles can be ignored in calibration, as it is only 0.45 %. However, the energy sensors do exhibit the characteristic of temperature effect. The experimental results presented in this study provide valuable insights for the analysis of laser calibration experimental data.

5. Acknowledgments

This work was supported by National Key R&D program of China (2021YFA0718403). The LHAASO project is supported by the Key Laboratory of Particle Astrophysics, Institute of High Energy Physics, CAS, the Joint Lab for Cosmic Ray Physics of Southwest Jiaotong University and the Institute of High Energy Physics, CAS. The authors would like to express their gratitude to Jiangbazhaxi, H. Q. Zhang, Silangdazhu, Angwangsilang, Ouzhu, and X. Li for their assistance in testing, operating, and maintaining the laser facilities.

References

[1] Wu Wenxiong, Zuo Xiong, Xiao Gang, et al., The performance test of LHAASO-MD photomultiplier [J]. Astronomical research & technology, 2020, 17(2):258-264.

[2] Ji Fang, Zhang Jianxin, Chen Mingjun, et al., Water Quality Monitoring Analysis Based on WCDA. Astronomical Research & Technology, 2020, 17(2) : 252-257.

[3] F. Aharonian, Q. An, Axikegu et al., Reconstruction of Cherenkov image by multiple telescopes of LHAASO-WFCTA. Radiat Detect Technol Methods 6, 544 (2022)

[4] Ma Xinhua, Bi Yujiang, Cao Zhen, et al., Chapter 1 LHAASO Instruments and Detector technology[J]. Chinese Physics C, 2022, 46(3) : 7-41.

[5] Sun Qinning, Chen Long, Liu Hu, et al., The YAG Lidar System Applied in LHAASO.Proceedings of 37th International Cosmic Ray Conference — PoS(ICRC2021).

[6] Yang Wang, Chen Long, Zhu Fengrong, et al., The Laser calibration system for LHAASO-WFCTA. Proceedings of 37th International Cosmic Ray Conference — PoS(ICRC2021).

[7] Chen Long, Wang Yang, Zhu Fengrong, et al., Application of the nitrogen laser calibration system in LHAASO-WFCTA. Proceedings of 37th International Cosmic Ray Conference — PoS(ICRC2021).

[8] Li Xinyu, Lu Shengguo, Chen Xiangzhong, et al., Pyroelectric and electrocaloric materials[J]. JOURNAL OF MATERIALS CHEMISTRY C, 2013, 1(1) : 23-37.